

Radiation Forces Constrain the FRB Mechanism

Pawan Kumar^{1*} and Wenbin Lu^{2†}

¹*Department of Astronomy, University of Texas at Austin, TX 78712, USA*

²*TAPIR, Walter Burke Institute for Theoretical Physics, Mail Code 350-17, Caltech, Pasadena, CA 91125, USA*

3 April 2020

ABSTRACT

We provide constraints on Fast Radio Burst (FRB) models by careful considerations of radiation forces associated with these powerful transients. We find that the induced-Compton scatterings of the coherent radiation by electrons/positrons accelerate particles to very large Lorentz factors (LF) in and around the source of this radiation. This severely restricts those models for FRBs that invoke relativistic shocks and maser type instabilities at distances less than about 10^{13} cm of the neutron star. Radiation traveling upstream, in these models, forces particles to move away from the shock with a LF larger than the LF of the shock front. This suspends the photon generation process after it has been operating for less than ~ 0.1 ms (observer frame duration). We show that masers operating in shocks at distances larger than 10^{13} cm cannot simultaneously account for the burst duration of 1 ms or more and the observed \sim GHz frequencies of FRBs without requiring an excessive energy budget ($> 10^{46}$ erg); the energy is not calculated by imposing any efficiency consideration, or other details, for the maser mechanism, but is entirely the result of ensuring that particle acceleration by induced-Compton forces upstream of the shock front does not choke off the maser process. For the source to operate more or less continuously for a few ms, it should be embedded in a strong magnetic field – cyclotron frequency \gg wave frequency – so that radiation forces don't disperse the plasma and shut-off the engine.

Key words: Radiation mechanisms: non-thermal - methods: analytical - stars: magnetars - radio continuum: transients - masers

1 INTRODUCTION

Fast radio bursts (FRBs) are milli-second-duration bright (flux density \sim Jansky) transient events observed between 400 MHz and 7 GHz frequencies (Amiri et al. 2019a, 2019b; Ravi 2019a, 2019b; Ravi et al. 2019; Osłowski et al. 2019; Kocz et al. 2019; Bannister et al. 2019; Gajjar et al. 2018; Michilli et al. 2018; Farah et al. 2018; Shannon et al. 2018; Bannister et al. 2017; Law et al. 2017; Chatterjee et al. 2017; Marcote et al. 2017; Tendulkar et al. 2017; Spitler et al. 2016; Petroff et al. 2016; Spitler et al. 2014; Thornton et al. 2013; Lorimer et al. 2007). Numerous mechanisms have been suggested for the generation of the coherent radio emission of FRBs, eg. Kumar et al. (2017), Metzger et al. (2017), Yang & Zhang (2018), Lu & Kumar (2018), Metzger et al. (2019); for recent reviews see Katz (2018), Petroff et al. (2019), Codes & Chatterjee (2019). Most of these mechanisms are proposed to operate at a distance from neutron star surface of 10^{13} cm or less. We explore in this paper constraints on the FRB radiation mechanisms provided by rapid acceleration of charge particles by the strong electric field associated with the radiation and induced Compton scatterings of photons; induced Compton scattering refers to the scattering of a photons by electrons when the occupation num-

ber of photon quantum states is much larger than unity (for FRBs the occupation number is of order 10^{35}). The electron-photon scattering optical depth is increased due to the induced-Compton effect, which has been calculated by many authors, e.g. Melrose (1971), Blandford (1973), Blandford & Scharlemann (1975), Wilson & Rees (1978). We include the constraint on FRB models provided by induced-Compton (IC) optical depth, but that turns out to much weaker than the IC acceleration that is estimated here. Particle acceleration due to the electric field of FRB radiations and its implications are considered in §2. Acceleration due to induced-Compton scatterings is described in §3, and the constraints these processes and some other general considerations impose on the FRB source and radiation mechanisms is discussed in §4.

2 PARTICLE MOTION DUE TO LARGE AMPLITUDE EM WAVE AND STATIC MAGNETIC FIELD

The RMS electric field strength associated with FRB radiation at a distance R from the source is

$$\frac{E_0}{\sqrt{2}} = \left(\frac{L}{cR^2} \right)^{1/2} = (1.8 \times 10^3 \text{ esu}) L_{43}^{1/2} R_{13}^{-1}, \quad (1)$$

where L is isotropic equivalent luminosity of the FRB. The non-linearity parameter, a , associated with this field – which is a rough

* pk@astro.as.utexas.edu

† wenbinlu@caltech.edu

measure of the energy gained by an electron traveling a distance of one wavelength in the wave-electric-field divided by its rest mass-energy – is

$$a \equiv \frac{qE_0}{mc\omega} = 4.5 L_{43}^{1/2} R_{13}^{-1} \omega_{10}^{-1}, \quad (2)$$

where q and m are electron charge and mass respectively, and ω is the wave frequency (radian s^{-1}).

Let us consider the motion of a particle exposed to a linearly polarized EM wave and a uniform magnetic field that is perpendicular to the wave-vector of the EM wave. The wave EM fields and vector potentials for the EM wave and the static magnetic field are as follows:

$$\mathbf{E}_w = E_0 \hat{x} \sin(kz - \omega t), \quad \mathbf{B}_w = E_0 \hat{y} \sin(kz - \omega t), \quad (3)$$

$$\mathbf{A}_w = -\frac{cE_0}{\omega} \hat{x} \cos(kz - \omega t), \quad \mathbf{A}_B = (B_y \hat{x} - B_x \hat{y})z. \quad (4)$$

The Lagrangian for particle motion is

$$L = -\frac{mc^2}{\gamma} + \frac{q}{c} \mathbf{A} \cdot \mathbf{v}, \quad (5)$$

where γ is the LF of the particle, \mathbf{v} is its 3-velocity, and $\mathbf{A} = \mathbf{A}_w + \mathbf{A}_B$ is the vector potential for the EM wave plus the static magnetic field. The x and y components of the particle's canonical momentum are conserved since the Lagrangian is independent of x and y coordinates–

$$p_x = m\gamma v_x + \frac{qA_x}{c} = m\gamma v_x - \frac{qE_0}{\omega} \cos \psi + \frac{qB_y z}{c} = \text{constant}, \quad (6)$$

$$p_y = m\gamma v_y - \frac{qB_x z}{c} = \text{constant}, \quad (7)$$

where

$$\psi = kz - \omega t. \quad (8)$$

The z -component of the momentum equation

$$\frac{d\gamma v_z}{dt} = \frac{q}{mc} [B_w v_x + v_x B_y - v_y B_x], \quad (9)$$

can be rewritten as

$$\frac{d}{dt} [\gamma v_z - \gamma c - \omega_B (x \sin \theta_B - y \cos \theta_B)] = 0, \quad (10)$$

where

$$\sin \theta_B = B_y/B, \quad \text{and} \quad \omega_B = \frac{qB}{mc} \quad (11)$$

is the cyclotron frequency.

We assume that the particle is initially at rest, i.e. $\mathbf{v} = \mathbf{0}$, before it is hit by the EM wave, and that its initial position is $\mathbf{r} = \mathbf{0}$. Thereafter its velocity is obtained from equations (6), (7) and (10) by applying the initial conditions,

$$\gamma v_x = ac [\cos(kz - \omega t) - 1] - \omega_B z \sin \theta_B, \quad (12)$$

$$\gamma v_y = \omega_B z \cos \theta_B, \quad (13)$$

$$\gamma v_z = c(\gamma - 1) + \omega_B (x \sin \theta_B - y \cos \theta_B), \quad (14)$$

where a is given by equation (2).

The particle LF is easily obtained from these equations and is

$$\gamma = \frac{4a^2 \sin^4(\psi/2) + 4a \sin^2(\psi/2) \xi_z \sin \theta_B + \xi_z^2 + 1}{2[1 - \xi_\rho \sin(\theta_B - \phi)]} + [1 - \xi_\rho \sin(\theta_B - \phi)]/2 \quad (15)$$

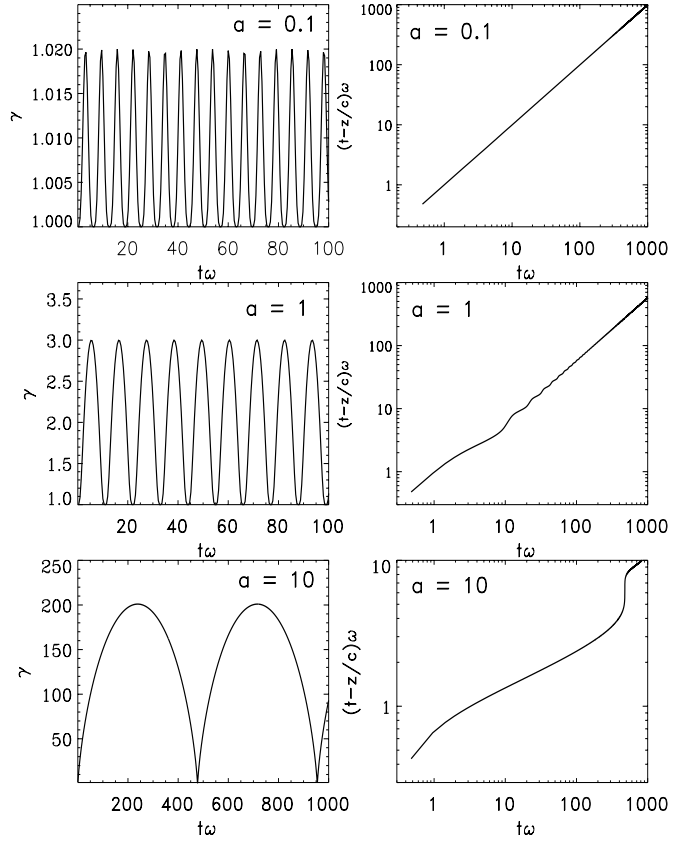


Figure 1. Shown on the left panels are the particle LF, γ , as a function of dimensionless time, $t\omega$, for three different values of a : 0.1, 1 and 10 (top to bottom); where ω is the EM wave frequency. These calculations are for weak magnetic fields such that the ratio of the electron cyclotron frequency and the EM wave frequency (ω_B/ω) is 10^{-5} ; results for $\omega_B/\omega = 10^{-3}$ are effectively the same as shown here. The three right panels show the location of the particle wrt the front of the EM wave, i.e. $[t - z(t)/c]\omega$; for large values of a , the particle rides the wave at a roughly constant phase angle for a long duration of time (see the bottom right panel for $a = 10$).

where

$$\sin \phi = y/\rho, \quad \rho^2 = x^2 + y^2, \quad \xi_\rho = \rho\omega_B/c, \quad \xi_z = z\omega_B/c. \quad (16)$$

The particular case of $\omega_B = 0$, i.e. vanishing static magnetic field, is illuminating:

$$\gamma v_x = -2ac \sin^2(\psi/2), \quad \gamma v_z = c(\gamma - 1), \quad \gamma = 1 + 2a^2 \sin^4(\psi/2). \quad (17)$$

For $a > 1$, the particle LF is of order $2a^2$ and its velocity vector lies within an angle $\sim a^{-1}$ of the wave propagation direction. For $a \ll 1$, the velocity component along the wave vector oscillates at frequency 2ω and perpendicular to it at frequency ω . However, for $a > 1$, the phase function along the particle worldline $|\psi| = \omega t - kz(t) \sim \omega t/2\langle\gamma^2\rangle$, and so the particle LF oscillates at frequency $\sim \omega/\langle\gamma^2\rangle \sim \omega/[2(1+a^2)]$; where $\langle\gamma^2\rangle$ is the time averaged LF-squared of the particle. Figure 1 shows numerical results for particle trajectories for a few different values of a .

Particles out to a very large distance from the source of the intense FRB radiation are vigorously agitated and forced to move at high velocities – the time averaged LF $\gamma \sim a^2 \sim 10^2 R_{13}^{-2}$; the non-

linearity parameter for those FRBs which emit a good fraction of their energy at ~ 500 MHz frequency is: $a \sim 10 R_{13}^{-1} L_{43}^{1/2}$ (see eq. 2).

Considering that charge particles are forced to move at close to the speed of light by the electric field of the radiation out to a distance $\sim 10^{14}$ cm from the source, it might be hard for the plasma lens model (Cordes et al. 2017; Main et al. 2018) to operate within this distance of the source – a few ms duration radiation pulse cannot pass through the plasma in the “lens” if the plasma is located at a distance $\lesssim 10^{13}$ cm from the FRB source since the plasma would be forced to move at speed $\sim c$ by the wave electric field – unless the magnification factor of the plasma lens is much larger than $\sim 10^2$.

If the FRB radiation is produced in shock heated plasma (e.g. Metzger et al. 2019) at radius R , then particles upstream of the shock front would be accelerated to LF $\gamma \approx 2a^2 \sim 50 L_{43} R_{13}^{-2} \omega_{10}^{-2}$ (eq. 2) by the electric field of radiation moving upstream as long as the composition of the medium is e^\pm and the cyclotron frequency is much less than 1 GHz. The LF of upstream particles wrt to the shock in this case is $\sim \gamma_{sf}/2\gamma$; γ_{sf} is the LF of the shock front wrt to the undisturbed, upstream, medium. The upstream medium is also compressed by a factor $\sim 4a^2$ due to this acceleration, and the component of upstream particle four-velocity tangential to the shock-surface is $\sim a$ which varies on a time scale of the wave period. These effects would modify the growth rate of synchrotron maser instability operating near the shock front, and reduce the efficiency of converting blast wave energy to coherent GHz radiation.

Furthermore, particle acceleration upstream of the shock front would shut off radiation production for a while in the observed band, if $R \lesssim 10^{13}$ cm, until upstream particles slow down by plowing into the plasma further out. So the radiation by shocked plasma is not going to be produced continuously if $R \lesssim 10^{13}$ cm.

Another effect of particle acceleration by the intense FRB radiation is that it depletes the energy from the the outward moving radiation front – charge particles undergoing acceleration radiate – at a rate much larger than one might expect from Thomson scatterings. This is estimated in the following sub-section, where we also discuss the constraints imposed by this process on the circum-burst medium.

2.1 Radiative loss of Wave-accelerated particles

We calculate in this sub-section the energy loss suffered by FRB pulse as it travels through the CSM of the magnetar due to power radiated by particles that are accelerated by the EM field of the FRB radiation (particle acceleration was calculated in §2). The power emitted by a relativistic particle undergoing acceleration is given by (the covariant form of) the Larmor formula

$$P = \frac{2q^2}{3c} \left[- \left(\frac{du^0}{d\tau} \right)^2 + \sum_{i=x,y,z} \left(\frac{du^i}{d\tau} \right)^2 \right], \quad (18)$$

where $(u^\mu) = \gamma(1, v_x, v_y, v_z)$ is the four-velocity and $d\tau = dt/\gamma$ is the differential proper time. The total emitted energy within the interaction time t_{int} is then given by $E_{rad} = \int_0^{t_{int}} P dt$, which is the amount of energy that is *spontaneously scattered* by the particle according to classical electrodynamics. In this picture, the scattered photons occupy very different regions of the phase space (for both frequency and direction) from the incoming photons, so we ignore stimulated emission (which will be discussed in the next section). We have checked that the radiative back-reaction force is negligible compared to the Lorentz force for the entire parameter space considered in this paper. However, as we show below, the cumulative energy loss could be significant such that a large fraction of the FRB wave energy

is scattered away. This in turn provides a constraint on the gas density of the FRB environment.

Consider the FRB waves propagating through a strongly magnetized relativistic wind with luminosity L_w and LF γ_w . An order unity fraction of the wind power is carried by Poynting flux and a fraction $\mu_w^{-1} < 1$ is carried by electron (and positron) kinetic energy flux. At radius R (much greater than the light cylinder of a neutron star), the magnetic field strength in the lab frame is $B \simeq \sqrt{L_w}/(r^2 c)$. For a pulse of duration t_{FRB} , the interaction time between a particle and the FRB wave is

$$t_{int} \simeq \min(R/c, \gamma_w^2 t_{FRB}). \quad (19)$$

We calculate the cumulative scattered energy for each electron in the wind comoving frame E'_{rad} and then Lorentz transform that to the lab frame $E_{rad} = \gamma_w E'_{rad}$. The total number of electrons participating in the interaction near characteristic radius R is

$$N_e \simeq \frac{L_w}{\mu_w \gamma_w m c^2} \max \left(\frac{R}{\gamma_w^2 c}, t_{FRB} \right). \quad (20)$$

If the total scattered energy exceeds the total wind energy $\mu_w N_e \gamma_w m c^2$, then the wind should be significantly accelerated by the photon momentum which decreases E_{rad} . Thus, the scattered energy should generally be written as

$$E_{sca} = N_e \min(E_{rad}, \mu_w \gamma_w m c^2). \quad (21)$$

Therefore, we obtain the ratio between scattered energy and the FRB wave energy

$$\frac{E_{sca}}{E_{FRB}} \simeq \frac{L_w}{L_{43}} \min \left(\frac{E_{rad}}{\mu_w \gamma_w m c^2}, 1 \right) \max \left(\frac{R_{13}}{3 \gamma_w^2 t_{FRB, -3}}, 10^{-6} \right). \quad (22)$$

Fig. 2 shows $\log(E_{sca}/E_{FRB})$ as a function of L_w and γ_w for a typical weak burst from FRB 121102. If the FRB source is within the magnetosphere of a neutron star (below the light cylinder), we ruled out the presence of a mildly relativistic ($\gamma_w \lesssim 10$) wind from the progenitor star with $L_w \gtrsim 10^{39}$ erg s $^{-1}$, regardless of its composition (pair or electron-proton), since the FRB pulse would lose a large fraction of its energy. We note that the persistent radio source associated with FRB 121102 (luminosity $\sim 10^{39}$ erg s $^{-1}$, at projected distance of < 40 pc, Chatterjee et al. 2017, Marcote et al. 2017) may still be powered by an ultra-relativistic $\gamma_w \gg 10$ wind like that in the Crab Nebula.

3 PARTICLE ACCELERATION DUE TO INDUCED COMPTON SCATTERINGS

In this section, we calculate particle acceleration by scattering photons when the occupation numbers of both the initial and the final photon states are very large, i.e. due to induced Compton (IC) scatterings. The calculations described here are valid when the wave nonlinearity parameter “ a ” (eq. 2) is less than 1; IC scatterings for highly nonlinear waves is a complicated problem and will be taken up in a future paper, however, nonlinear effects when $a > 1$ are included in numerical calculations presented in Fig. 3.

It is best to view the process from the rest frame of an electron. A photon of wave-vector \mathbf{k}' is scattered to \mathbf{k}'_1 in electron rest frame. The momentum kick given to the electron in this scattering is $\mathbf{k}' - \mathbf{k}'_1$. The inverse of the process where $(k_2 \hat{\mathbf{k}}_1) \rightarrow \mathbf{k}'$ gives an almost exact opposite kick to the electron; $\hat{\mathbf{k}}'_1 \equiv \mathbf{k}'_1/|\mathbf{k}'_1|$ is a unit vector. The non-zero difference between the two is due to the electron recoil in this scattering process so that $k'_1 \neq k'$.

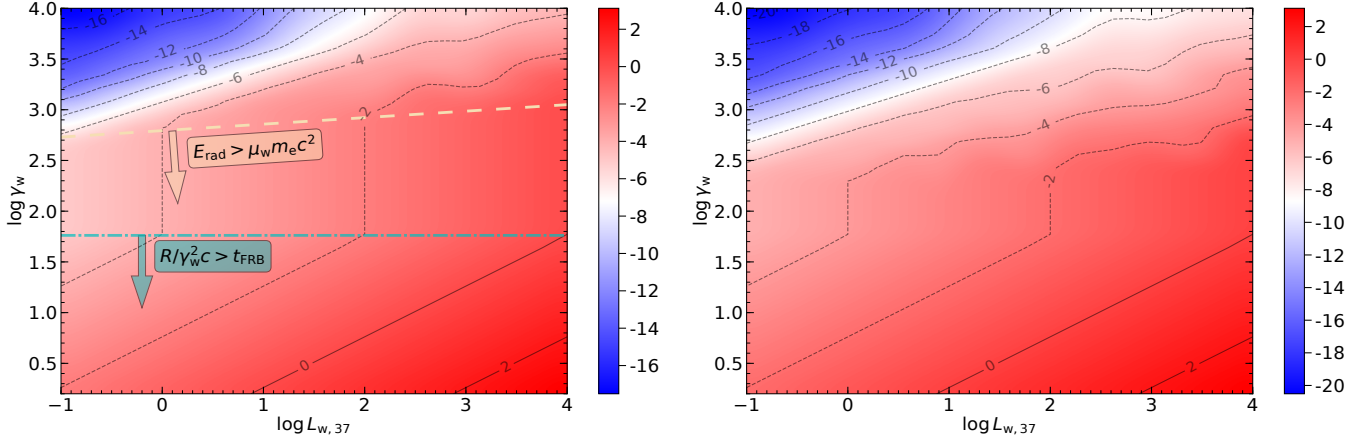


Figure 2. The ratio between scattered energy and FRB energy $\log(E_{sca}/E_{FRB})$ as a function of wind power $L_w = 10^{37} L_{w,37} \text{ erg s}^{-1}$ and LF γ_w . The region with $\log(E_{sca}/E_{FRB}) > 0$ is ruled out. We consider a typical weak burst from FRB 121102 with $t_{FRB} = 0.1 \text{ ms}$ and $L = 10^{41} \text{ erg s}^{-1}$ at $\nu = 1 \text{ GHz}$. We assume the source to be located much below the light cylinder of a neutron star ($\ll 10^{10} \text{ cm}$) and take the characteristic FRB-wind interaction radius to be $R = 10^{10} \text{ cm}$. The left panel is for $\mu_w = 1$ (corresponding to magnetized e^\pm wind), and the right panel is for $\mu_w = 10^3$ (magnetized electron-proton wind). The thick dashed and dash-dotted lines on the left panel mark the different regimes of the parameter space (see eq. 22). Note that the particle trajectory for $\omega_B \gg \omega$ and $a \gg 1$ is chaotic, and we have carried out convergence tests with different time resolutions to confirm the qualitative results.

The rate of momentum transfer to an electron by a narrow beam of photons with wave-vector within $d^3 k'$ and its inverse process is

$$\delta \mathbf{p}' = \frac{c\hbar}{2} \frac{d\sigma_T}{d\Omega_{\chi'}} \left[(1 + n_{\mathbf{k}'_1}) n_{\mathbf{k}'} (\mathbf{k}' - \mathbf{k}'_1) \frac{d^3 k'_1}{4\pi^3} + (1 + n_{\mathbf{k}'_2}) n_{\mathbf{k}'_2} (\mathbf{k}'_2 - \mathbf{k}') \frac{d^3 k'_2}{4\pi^3} \right] d\Omega_{\chi'}, \quad (23)$$

where

$$\cos \chi' \equiv \hat{\mathbf{k}}' \cdot \hat{\mathbf{k}}'_1, \quad k'_1 = k' - \Delta k', \quad k'_2 = k' + \Delta k',$$

$$dk'_2 = dk' (1 + 2\Delta k'/k'), \quad \text{and} \quad \hbar \Delta k' = \frac{\hbar^2 k'^2}{mc} (1 - \cos \chi') \quad (24)$$

is the momentum recoil suffered by the electron due to scattering one photon of momentum $\hbar \mathbf{k}'$ by an angle χ' . The factor $4\pi^3$ in the denominator in equation (23) is because the number of distinct photon quantum states in volume $d^3 k'$ is $d^3 k'/4\pi^3$.

We are considering the case where $n_{\mathbf{k}} \gg 1$ is a function of $|\mathbf{k}|$ within a cone, in the \mathbf{k} -space, of opening angle $\theta_s \ll 1$. Expressing k'_1 and k'_2 in terms of k' (eq. 24), and Taylor expansion of $n_{\mathbf{k}'_1}$ & $n_{\mathbf{k}'_2}$ in terms of $n_{\mathbf{k}'}$, transforms equation (23) to the following expression

$$\delta \mathbf{p}' = \frac{d\sigma_T}{d\Omega_{\chi'}} \frac{\hbar k'^3 dk' d\Omega_{\chi'}}{4\pi^3} \left[(\hat{\mathbf{k}}' - \hat{\mathbf{k}}'_1) d\Omega_{\mathbf{k}'} - (\hat{\mathbf{k}}' - \hat{\mathbf{k}}'_1) d\Omega_{\mathbf{k}'_1} + \frac{\Delta k'}{k'} (\hat{\mathbf{k}}'_1 d\Omega_{\mathbf{k}'} + \hat{\mathbf{k}}'_1 d\Omega_{\mathbf{k}'_1}) + \frac{2(\mathbf{k}'_1 - \mathbf{k}') \Delta k'}{k'} \frac{\partial (n_{\mathbf{k}'_1} k'^2)}{k'_1 n_{\mathbf{k}'_1} \partial k'_1} d\Omega_{\mathbf{k}'_1} \right] c n_{\mathbf{k}'} n_{\mathbf{k}'_1} \quad (25)$$

Integrating the above expression over incident and scattered photon directions ($\Omega_{\mathbf{k}'}$ & $\Omega_{\mathbf{k}'_1}$) and frequency yields the total rate of momentum deposit to the electron by the induced-Compton scatterings. The $d\Omega_{\mathbf{k}'}$ and $d\Omega_{\mathbf{k}'_1}$ integrals, nested inside the square bracket in eq. (25), are carried out subject to the condition that the scattering angle χ' is held fixed. Thus, the first two terms in the square bracket cancel exactly when the angular integral over photon propagation direction is performed. The integral of the last term over $\Omega_{\mathbf{k}'_1}$ is smaller than the third term by at least a factor $\theta_s'^{-2}$ (θ_s' is half of angular size of the

radiation beam in the electron rest frame). This is because both the incident and scattered photons lie within the angle θ_s' for the induced-Compton scattering¹ to be relevant and therefore, $|\mathbf{k}'_1 - \mathbf{k}'| \lesssim k' \theta_s'^2/2$. Thus, the last term in equation (25) can be ignored as well. This simplifies the expression for the radiation force on the electron considerably

$$\frac{d\mathbf{p}'}{dt'} \approx \frac{c\hbar}{2\pi^3} \int dk' k'^2 \int d\Omega_{\chi'} \frac{d\sigma_T}{d\Omega_{\chi'}} \int d\Omega_{\mathbf{k}'} \hat{\mathbf{k}}'_1 \Delta k' n_{\mathbf{k}'} n_{\mathbf{k}'_1}. \quad (26)$$

Since $k' - k'_1 = \Delta k' \ll k'$ (see equation 24), we can take $n_{\mathbf{k}'_1} \approx n_{\mathbf{k}'}$, and the integral over $\Omega_{\mathbf{k}'}$ gives $(\pi \theta_s'^2 \Delta k' n_{\mathbf{k}'}) \hat{\mathbf{z}}$; the axis of the photon beam cone is along $\hat{\mathbf{z}}$, and the photon occupation number ($n_{\mathbf{k}'}$) is taken to be angle-independent inside the radiation cone, i.e. for $\theta' < \theta_s'$. Thus, equation (26) reduces to

$$\frac{d\mathbf{p}'}{dt'} \approx \frac{3\hbar^2 \sigma_T \theta_s'^2}{4\pi^2 m} \int dk' k'^4 n_{\mathbf{k}'}^2 \int_0^{\theta_s'} d\chi' \sin \chi' \sin^2 \Theta' \times \sin^2(\chi'/2) \hat{\mathbf{z}}, \quad (27)$$

where we made use of equation (24) for $\Delta k'$ and

$$\frac{d\sigma_T}{d\cos \chi'} = \frac{3\sigma_T}{4} \sin^2 \Theta', \quad (28)$$

which is the differential scattering cross-section of an electron for linearly polarized radiation; where Θ' is the angle between the electric vector of incident radiation and the momentum vector of scattered photons in the electron rest frame ($\Theta' \approx \pi/2$ for small angle scatterings that are relevant for IC acceleration).

The final two integrals are straightforward and are carried out assuming that $\theta_s' \ll 1$ and $n_{\mathbf{k}'}$ is a smooth function of k' :

$$\frac{d\mathbf{p}'}{dt'} \approx \frac{3\hbar^2 \sigma_T \theta_s'^6 k'^5 n_{\mathbf{k}'}^2}{64\pi^2 m} \quad (29)$$

We can transform this equation to lab frame by noting that $dp'_z/dt' =$

¹ Scattering a photon outside the radiation beam ($\chi' \gtrsim \theta_s'$) is a weaker process than the induced Compton within the beam for the FRB parameters being considered here.

dp_z/dt since the Lorentz boost is in the same direction as $\delta\mathbf{p}'$ and the change to the particle energy in the comoving frame is proportional to $|\delta\mathbf{p}'|^2$. Moreover,

$$\begin{aligned} \sin\theta'_s &= \frac{\sin\theta_s}{\gamma(1-\beta\cos\theta_s)} \approx 2\gamma\theta_s, \quad \text{for } (\theta_s\gamma) \ll 1, \\ k' &= k\gamma(1-\beta\cos\theta_s) \approx k/2\gamma \quad \text{for } (\theta_s\gamma) \ll 1, \end{aligned} \quad (30)$$

which leads to

$$\frac{dp_z}{dt} \approx \frac{3\hbar^2\sigma_T\theta_s^6k^5\gamma n_{k'}}{32\pi^2m}. \quad (31)$$

The photon occupation number, $n_{k'}$, is a Lorentz invariant quantity and it can be easily shown to be

$$n_k = \frac{c^2L_\nu}{8\pi^2\theta_s^2R^2h\nu^3} \sim \frac{c^2L}{8\pi^2\theta_s^2R^2h\nu^4} \quad (32)$$

where L_ν is the specific luminosity (isotropic equivalent), R is distance from the FRB source where particle acceleration is being considered. Substituting this into equation (31) we finally obtain

$$\frac{dp_z}{dt} \approx \frac{3\sigma_T\theta_s^2L^2\gamma}{256\pi^3R^4\nu^3mc}. \quad (33)$$

If the inertia of the medium is dominated by electrons and positrons then $p_z = mc\beta\gamma$, and the equation for LF of the particle is

$$\frac{d\beta\gamma}{dt} \approx \frac{3\sigma_T\theta_s^2L^2\gamma}{256\pi^3R^4\nu^3m^2c^2}. \quad (34)$$

This result is easy to understand as follows. Since for induced-Compton scatterings, the scattered photon lies within the photon beam of opening angle θ'_s , the scattering cross-section is $\sigma_T\theta_s'^2 n_k$. In each scattering, the electron is recoiled and the momentum impulse it receives – when we subtract the contribution from its inverse process – is $\sim h^2\nu'^2\theta_s'^2/(2mc^3)$. The number of photons streaming outward per unit area and time is, $L'/(4\pi R^2h\nu')$. Combining all of these pieces we find the radiative force on an electron to be, $\sigma_T L n_k h\nu\theta_s'^4\gamma/(8\pi R^2m^2c^3)$; where we made use of Lorentz transformations, i.e. $\theta'_s \sim \gamma\theta_s$, $\nu' \sim \nu/\gamma$, $L' \sim L/\gamma^2$. Substituting for n_k from equation (32) we arrive at an expression for the radiative force on the electron that is within a factor 2 of that given in equation (33). It should be noted that particle acceleration is more severe when the medium through which the coherent radiation propagates is moving away from the source at relativistic speeds.

4 CONSTRAINTS ON FRB RADIATION MECHANISMS

We consider two cases in separate sub-sections. The first one is where the magnetic field in the source is weak, $B \lesssim 10^3\text{G}$, so that the cyclotron frequency is less than 1 GHz and the scattering of FRB radiation is not affected by the magnetic field. The other case is that of a strong magnetic field which is analyzed in §4.2.

4.1 The medium through which the FRB radiation is passing has weak magnetic field (cyclotron frequency \lesssim GHz)

The FRB scenario considered in this section is where the coherent radiation is produced when a relativistic jet from a compact object interacts with the circum-stellar medium (CSM) and a fraction of the jet energy is converted to GHz photons. We provide general constraints on the viability of this model.

The ability of the shock model to reproduce the observed duration of FRBs, and their frequency can be robustly constrained by

combining a few physical considerations. For much of the following discussions we will ignore factors of order unity.

If the FRB radiation were to be produced at radius $\lesssim 10^{13}\text{cm}$, the nonlinear parameter associated with the radiation at this radius is $a \gtrsim 5$ (eq. 2) and electrons upstream of the shock front are accelerated to $LF\ 2a^2 \gtrsim 50$ (see §2). This high LF of particles upstream completely changes the shock dynamics as well as the cyclotron/synchrotron maser instability growth rate that has been suggested for FRB radiation (Plotnikov & Sironi 2019). Furthermore, induced Compton scatterings upstream of the shock front provide important constraint on the shock model for FRB radiation.

The induced-Compton (IC) scattering optical depth ahead of the shock front is given by (e.g. Lyubarsky 2008, Lu & Kumar 2018)

$$\tau_{ic} \sim \frac{\sigma_T L n_w (ct_{FRB})}{8\pi^2 R^2 m \nu^3} \sim \frac{4L_{43} n_w 2t_{FRB,-3}}{R_{13}^2 \nu_9^3} \quad (35)$$

This equation is valid for both IC scatterings within the photon beam and outside the photon beam as long as $R \sim 2ct_{FRB}/\theta_s^2$, where θ_s is the beam size of the coherent radiation at R (the shock radius) – $\theta_s \approx \gamma_{sw}^{-1}$ when the radiation is produced in a relativistic shock and the LF of the shocked fluid wrt the upstream unshocked plasma is γ_{sw} . The IC optical depth given in equation (35) is in the CSM rest frame. We need to modify this equation if the upstream CSM is a wind with LF γ_w . The luminosity in the wind rest frame $L' \approx L/\gamma_w^2$, $\nu' \approx \nu/\gamma_w$, and the burst duration in the wind frame is $t'_{FRB} \approx \gamma_w^2 t_{FRB}$. Thus, the IC optical depth can be rewritten as

$$\tau_{ic} \sim \frac{\sigma_T L' n'_w (ct'_{FRB})}{8\pi^2 R^2 m \nu'^3} \sim \frac{\sigma_T L L_w \gamma_w (ct_{FRB})}{32\pi^3 m^2 c^3 \mu_w R^4 \nu^3}, \quad (36)$$

where L_w and μ_w are wind luminosity and magnetization parameter, and we used the relation $L_w = 4\pi R^2 n'_w m c^3 \mu_w \gamma_w^2$ to get rid of n'_w . The requirement that $\tau_{ic} < 1$ provides an upper bound on the CSM density

$$n_w(R) = n'_w \gamma_w \lesssim (30\text{cm}^{-3}) \frac{R_{13}^2 \nu_9^3}{L_{43} t_{FRB,-3} \gamma_w^2}. \quad (37)$$

For density $n_w \ll 10\text{cm}^{-3}$, the relativistic jet deceleration radius and the place where coherent radiation is produced is $\gtrsim 10^{13}\text{cm}$ (see §4.1.1). This alleviates the problem associated with the acceleration of upstream e^\pm away from the shock front to high LF due to the electric field of the coherent FRB radiation. Moreover, at the larger radius, particle acceleration due to induced Compton scatterings also poses less of a problem as we describe next. However, the frequency of maser photons produced in the shock is below the observing band for even CHIME at this low CSM density; this point is discussed further in §4.1.1.

The LF of plasma upstream of the shock front – accelerated by induced-Compton scatterings of FRB radiation – can be calculated using equation (34), which is rewritten below for the relativistic case in a more convenient form

$$\begin{aligned} \frac{d\gamma}{dt} &= \frac{\gamma}{t_{acc}}, \quad \text{where} \\ t_{acc} &\sim \frac{256\pi^3 R^4 \nu^3 m^2 c^2}{3\sigma_T \theta_s^2 L^2} \sim (3 \times 10^{-13}\text{s}) \frac{R_{13}^4 \nu_9^3}{L_{43}^2 \theta_s^2}. \end{aligned} \quad (38)$$

This shows that the LF of particles increases exponentially on a very short time scale, and they attain a terminal LF of $\sim 3\theta_s^{-1} \approx 3\gamma_{sw}$ when the radiation field in the particle comoving frame becomes nearly isotropic and little momentum is imparted to electrons in further scatterings. If the cold upstream medium moves away from the source with LF γ_w then t_{acc} is smaller by a factor γ_w in the lab frame.

The leading front of the radiation that is produced by the

shock wave is ahead of the shock by a distance² $\sim \delta R/(2\gamma_{sw}^2) \sim ct_{FRB}(\delta R/R)$; where δR is the distance the shock has traveled since the onset of the radiation. Thus, the time available in the lab frame for an upstream particle to be accelerated to $\gamma \sim \gamma_{sw}$ by the radiation front before it is swept up by the shock is roughly $t_{FRB}/5$. This defines a radius, R_{ra} , beyond which radiative acceleration can be ignored. This radius is determined from the condition that $t_{acc} \sim t_{FRB}/10$:

$$R_{ra} \sim (5.5 \times 10^{13} \text{ cm}) t_{FRB,-3}^{2/5} L_{43}^{2/5} \nu_9^{-3/5}, \quad (40)$$

where we took $\theta_s \sim \gamma_{sw}^{-1}$, and $\gamma_{sw}^2 \sim R_{ra}/(2ct_{FRB})$ (see eq. 49). We note that R_{ra} depends extremely weakly on the effective particle inertia (per electron) as $R_{ra} \propto m_{eff}^{-1/5}$. Therefore, R_{ra} given by eq. (40) does not change by more than a factor 4 even if the inertial of the upstream plasma is dominated by ions or magnetic field instead of e^\pm . We also note that R_{ra} is larger by a factor $\gamma_w^{3/5}$ when the CSM upstream of the coherent source is moving away with LF γ_w .

If FRB radiation is produced when the shock front is at $R \lesssim R_{ra} \sim 10^{14}$ cm, then the e^\pm plasma upstream of the shock is accelerated to LF of order $3\gamma_{sw}$ due to the induced-Compton scattering of the radiation. Since the upstream particle velocity is larger than the shock front speed, and directed away from it, the effect of the IC scatterings is to prevent particles from approaching the front. Thus, radiation produced by the shock for a time much less than t_{FRB} , traveling upstream, accelerates plasma away from it, and halts further production of radiation. IC accelerated particles slow down as they move outward and share their momenta with a larger number of particles. However, even the swept up medium has relativistic speed up to a distance $[\tau_{ic}\delta E/4\pi nmc^2]^{1/3} \sim 5 \times 10^{13}$ cm $[\tau_{ic}(\delta E)_{38}/n_2]^{1/3}$ from the shock front; where δE is the energy of the radiation pulse produced by the shock before the process is shut off, and τ_{ic} is the optical depth of the CSM to IC scatterings out to the distance 5×10^{13} cm (given by eq. 35). We see that just 1% of a typical FRB radiation produced at $R \lesssim 10^{14}$ cm can drive CMS to speed $\sim c$ and halt the radiation production process.

4.1.1 Constraining maser mechanisms in shocks for FRB radiation

Let us consider that the relativistic jet from a compact object interacts with a cold wind with the following properties: the wind is composed of particles of mass m , has LF γ_w , its magnetization parameter (the ratio of magnetic to particle kinetic energy densities) is μ_w , energy density in wind comoving frame is u'_w , and its luminosity in lab frame is $L_w \approx 4\pi R^2 u'_w \gamma_w^2 c$. Similarly, the parameters of the relativistic jet are: γ_j , μ_j , u'_j and L_j . Let us take the LF of the shocked wind plasma wrt the unshocked wind to be γ_{sw} , and the shocked jet plasma LF wrt the unshocked jet fluid is γ_{sj} . It can be shown using the continuity of mass, momentum and energy flux across the shock front that for a relativistic, magnetized plasma, the energy density of the shocked wind (in shocked fluid rest frame) is $u'_{s,wind} \approx \gamma_{sw}^2 u'_w$, and similarly $u'_{s,jet} \approx \gamma_{sj}^2 u'_j$ (e.g. Kennel & Coroniti, 1984). The pressure equilibrium between the two shocked fluids, which are separated by the contact discontinuity surface, for highly relativistic systems, requires

² This assumes that the wave frequency, ω , is at least a factor few times γ_{sw} larger than the plasma frequency in the upstream medium. This is the situation with many FRB radiation production scenarios including the cyclotron/synchrotron maser instability mechanism that operates in the shock transition layer and downstream of the shock front. If this condition were not satisfied then the FRB radiation would not be able to travel away from the shock front to be received by the observer.

$u'_{s,jet} = u'_{s,wind}$. Moreover, the LF of the jet wrt the wind $\sim \gamma_j/\gamma_w$, should be equal to $\sim \gamma_{sj}\gamma_{sw}$, i.e. two different ways of calculating the relative speed of the jet and the wind should agree. Combining these two relations we find

$$\gamma_{sw}^4 \approx \frac{\gamma_j^2 u'_j}{\gamma_w^2 u'_w} \quad \text{or} \quad \gamma_{sw} \approx \left[\frac{L_j}{L_w} \right]^{1/4}. \quad (41)$$

The deceleration radius of the jet is the distance it travels before half of its energy is transferred to the circum-stellar medium. The total energy of the shocked wind, in the lab frame, is $\sim 4\pi R^3 u'_w \gamma_{sw}^2$. Thus, the deceleration radius is

$$E_j \equiv L_j t_{jet} \approx 8\pi R_{da}^3 u'_w \gamma_{sw}^2 \implies R_{da} \approx \frac{c E_j \gamma_w^2}{2 L_w \gamma_{sw}^2}, \quad (42)$$

where t_{jet} is the time duration in the lab frame over which the relativistic jet was launched from radius R_{jet} in the magnetosphere of the magnetar. The Shock LF after the deceleration radius is given by the energy conservation equation (42):

$$\gamma_{sw}(R > R_{da}) \approx \gamma_{sw}(R_{da}) \left[\frac{R}{R_{da}} \right]^{1/2}. \quad (43)$$

The FRB lasts for a time duration of order the jet deceleration time in the observer frame, t_{da}^{obs} , when roughly 50% of the coherent radiation is generated. The observer frame deceleration time can be calculated from R_{da} and LF of the shock front in the lab frame³, $\gamma_{sw} \mu_w^{1/2} \gamma_w$, using the standard formula for a source that is moving toward the observer with relativistic speed, e.g. Kumar & Zhang (2015)

$$t_{da}^{obs} \approx \frac{R_{da}}{2c [\gamma_{sw} \gamma_w \mu_w^{1/2}]^2} \approx \frac{t_{jet}}{4\mu_w}, \quad (44)$$

where we used equations (41) and (42) to arrive at the second equality in (44). The jet launching time, t_{jet} , ought to be smaller than a few ms because of FRB energetics⁴. Thus, the shock model gives burst duration (eq. 44) much smaller than the observed few ms width of FRBs if the magnetization parameter of the wind into which the relativistic jet is running into (μ_w) is larger than order unity. The possibility that the FRB radiation might be produced at a radius much larger than R_{da} will be considered later in this sub-section; the constraint on μ_w when $R \gg R_{da}$ turns out to be similar. It should also be noted that upstream particles are accelerated by IC scatterings more rapidly and out to larger distances when $\gamma_w \gg 1$ as discussed in §4.1, and that is an additional constraint on γ_w and μ_w .

Substituting for γ_{sw} from equation (44) into (42), and expanding $L_w \approx 4\pi R_{da}^2 \mu_w m c^3 \langle n'_w \rangle \gamma_w^2/3$, we find

$$R_{da} \sim \left[\frac{3E_j t_{FRB} \gamma_w^2}{4\pi m c \langle n'_w \rangle} \right]^{1/4} \sim (5 \times 10^{12} \text{ cm}) \gamma_w^{1/2} \left[\frac{E_{42} t_{FRB,-3}}{\langle n'_w \rangle_4} \right]^{1/4}, \quad (45)$$

where $\langle n'_w \rangle$ is the mean CSM particle number density in its rest frame

³ The Lorentz factor of the shock front is larger than the LF of the shocked plasma (γ_{sw}) by a factor $\sim \mu_w^{1/2}$ (e.g. Kennel & Coroniti, 1984).

⁴ The total energy of the relativistic jet (isotropic equivalent) for a typical FRB is of order 10^{42} erg if the radiation production efficiency is a few percent. Considering the ms duration of FRBs, the jet energy has to come from the magnetic field and not the neutron star rotation; the rate of energy extraction for the latter is set by the dipole radiation formula and is far smaller than what we see for FRBs (see eq. 51). For a magnetar with surface magnetic field of 10^{15} G, the total magnetic energy above the radius R is $2 \times 10^{42} R_8^{-3}$ erg. Therefore, the jet has been launched at a radius no larger than $\sim 10^8$ cm, i.e. $R_{jet} \lesssim 10^8$ cm and $t_{jet} \approx R_{jet}/c \lesssim 3$ ms.

within R_{da} ; $\langle n'_w \rangle = 3n'_w(R_{da})$ for a steady wind CSM. This expression is independent of the LF of the relativistic jet, and the magnetization of the wind. The second part of equation (45) is obtained by taking the average particle mass in the wind to be the electron mass; R_{da} is smaller for an ionic wind by a factor 7. Considering the weak dependence of R_{da} on burst energy and CSM density, it is hard for the FRB source, according to the shock model scenario, to be at a radius very different from 10^{13} cm. However, upstream particle acceleration by the emergent radiation renders the shock model not viable at $R \lesssim 10^{13}$ cm.

As argued before, the magnetization parameter of the wind CSM cannot be larger than order unity otherwise the FRB duration, according to the shock model, would be much smaller than the observed duration. Thus, we take $\mu_w \sim 1$. Moreover, the asymptotic LF of a magnetized wind satisfies the relation $\gamma_w \sim \mu_w^{1/2}$ (Goldreich & Julian, 1969; Granot et al. 2011). So we take γ_w to be of order unity as well. Thus, the expected CSM particle density at $R_{da} \sim 10^{13}$ cm, for an electron-positron wind, is

$$n_w \sim \frac{L_w}{4\pi R^2 m c^3} \sim (3 \times 10^5 \text{ cm}^{-3}) L_{w,37} R_{13}^{-2}, \quad (46)$$

where our choice of wind luminosity of 10^{37} erg s $^{-1}$ is for a young magnetar (see eq. 51). The high particle density upstream of the shock front makes the CSM highly opaque to induced-Compton scattering (eq. 35), and that is another problem with the shock model for FRB radiation.

FRB radiation could be generated in shocks at $R \gtrsim 10^{14}$ cm, where upstream particles are not forced by the radiation to move at relativistic speed away from the shock front. However, if we demand that $R \sim R_{da}$, so that the FRB radiation is produced efficiently, then that requires the energy of the relativistic jet to be $\gtrsim 10^{46}$ erg or $n \lesssim 1 \text{ cm}^{-3}$ (see eq. 45). The large energy requirement seems problematic especially for the repeater FRB 121102; the total energy of outbursts in the last 10 years for this object exceeds the available energy in magnetic fields of even an extreme magnetar if each outburst has $\gtrsim 10^{46}$ erg energy. On the other hand, if we take the CSM density to be sufficiently small so that $R_{da} \gtrsim 10^{14}$ cm then the frequency of coherent radio emission produced in shocks is much smaller than the observed frequencies for FRBs (this point is amplified below).

We next explore the possibility that the FRB radiation is generated at a radius $R_s \gtrsim 10^{14}$ cm, and relax the efficiency considerations so that R_s can be much larger than the deceleration radius (R_{da}) of the relativistic jet.

The characteristic photon frequency for many maser instabilities in plasmas is of order the plasma or cyclotron frequency depending on the nature of the instability (the latter is $\mu_w^{1/2}$ times the former; $\mu_w \equiv B^2/(8\pi n_w m c^2)$ is plasma magnetization parameter). The cyclotron frequency in the shocked wind frame is

$$\nu'_B \approx \frac{qB'_w}{2\pi m c}, \quad (47)$$

and in the observer frame it is

$$\nu_B \approx \nu'_B \gamma_{sw} \gamma_w \sim \frac{qL_w^{1/2} \gamma_{sw}}{2\pi m R_s c^{3/2}}. \quad (48)$$

We can eliminate γ_{sw} using the FRB duration for the shock model, viz.

$$t_{FRB} \approx \frac{R_s}{2c(\gamma_{sw} \gamma_w \mu_w^{1/2})^2}, \quad (49)$$

where the factor μ_w in the denominator is because the shock front LF wrt to the unshocked wind is $\gamma_{sw} \mu_w^{1/2}$ (the LF of shocked plasma wrt

the unshocked wind is γ_{sw}). Thus, we arrive at the following expression for the cyclotron frequency of the shocked wind in the observer frame (which should be of order the FRB frequency for any maser mechanism apart for a possible factor $\sim \mu_w^{1/2}$):

$$\nu_B \approx \frac{qL_w^{1/2} t_{FRB}^{-1/2}}{2^{3/2} \pi m c^2 R_s^{1/2} \gamma_w \mu_w^{1/2}} \approx (7 \times 10^8 \text{ Hz}) \frac{L_{w,37}^{1/2} t_{FRB,-3}^{-1/2}}{R_{s,14}^{1/2} \gamma_w \mu_w^{1/2}}. \quad (50)$$

This frequency is at the lower end of the radio band at which FRBs are observed. We see from the above equation that there is little room for $\gamma_w \mu_w^{1/2}$ to be much larger than order unity unless $L_w \gg 10^{37}$ erg s $^{-1}$.

The dipole wind luminosity for a 30 year old magnetar with surface field strength of 10^{15} G is (e.g. Goldreich & Julian, 1969)

$$L_w \sim 10^{37} \text{ erg s}^{-1} B_{NS,15}^{-2} t_9^{-2}, \quad (51)$$

as long as t is larger than the spin-down time t_{sd} , which is given by

$$t_{sd} \approx 500 \text{ s } B_{NS,15}^{-2} P_{-3}^2, \quad (52)$$

where P_{-3} is the pulsar rotation period in unit of 10^{-3} s. The luminosity is roughly constant for $t \lesssim t_{sd}$.

The maximum dipole wind luminosity at time t after the birth of a NS is

$$L_w^{max} \sim 10^{39} \text{ erg s}^{-1} P_{-1}^{-2} t_9^{-1}, \quad (53)$$

which corresponds to $t_{sd} \sim t$, and the surface magnetic field of

$$B \sim (7 \times 10^{13} \text{ G}) P_{-1} t_9^{-1/2}. \quad (54)$$

where P_{-1} is the pulsar rotation period in unit of 0.1 s at time t .

It is entirely possible that the pulsar magnetic field, especially for a young system, is highly non-dipolar. Moreover, the magnetar wind might not be rotationally powered, but instead launched by magnetic field dissipation. For these cases, the wind luminosity provided by equations 51–53 does not apply, and for that reason we consider L_w as high as 10^{40} erg s $^{-1}$ in all of our numerical calculations presented in Fig. 3.

The electron density associated with the magnetar e^\pm wind at R_s is $n_w \sim L_w/(4\pi R_s^2 m c^3 \gamma_w \mu_w) \sim 3 \times 10^3 \text{ cm}^{-3} L_{w,37} R_{s,14}^{-2} (\gamma_w \mu_w)^{-1}$. The density marginally exceeds the upper limit given in equation (37) – to avoid the medium upstream of the shock-front to become opaque to induced Compton scatterings – unless $\gamma_w \mu_w \gg 1$.

The LF of the shock at $R_s \gtrsim 10^{13}$ cm should be $\gtrsim 10^3 \gamma_w^{-1} \mu_w^{-1/2}$ in order to produce a ms duration burst (eq 49). This requires the luminosity of the relativistic jet, obtained from equation (41), to be $L_j \sim L_w \gamma_{sw}^4 \gtrsim 10^{49} \gamma_w^{-4} \mu_w^{-2} L_{w,37} \text{ erg s}^{-1}$.

The allowed parameter space for the maser-in-shocks model of FRB is shown in Figure 3. The parameters are for a FRB with observed luminosity of 2×10^{43} erg s $^{-1}$ (top three panels), which corresponds to the low end of the luminosity of non-repeaters (e.g. Luo et al. 2018; Ravi 2019). And the lower three panels of Figure 3 show results for radio luminosity of 3×10^{42} erg s $^{-1}$ which is the median luminosity for bursts of the repeater FRB 121102 (e.g. Michilli et al. 2018; Hessels et al. 2019). The observed luminosity is used for the calculation of particle acceleration upstream of the shock front, and for no other aspect of the maser mechanism. As the left top and bottom panels of the figure show, the energy requirement for maser-in-shock model grows very rapidly with increasing t_{FRB} . For bursts of duration longer than ~ 2 ms, $L_j \gtrsim 10^{49}$ erg s $^{-1}$. The energy requirement is reduced if the FRB frequency is much larger than the cyclotron frequency ν_B considered in these calculations.

There are no solutions when the relativistic jet luminosity

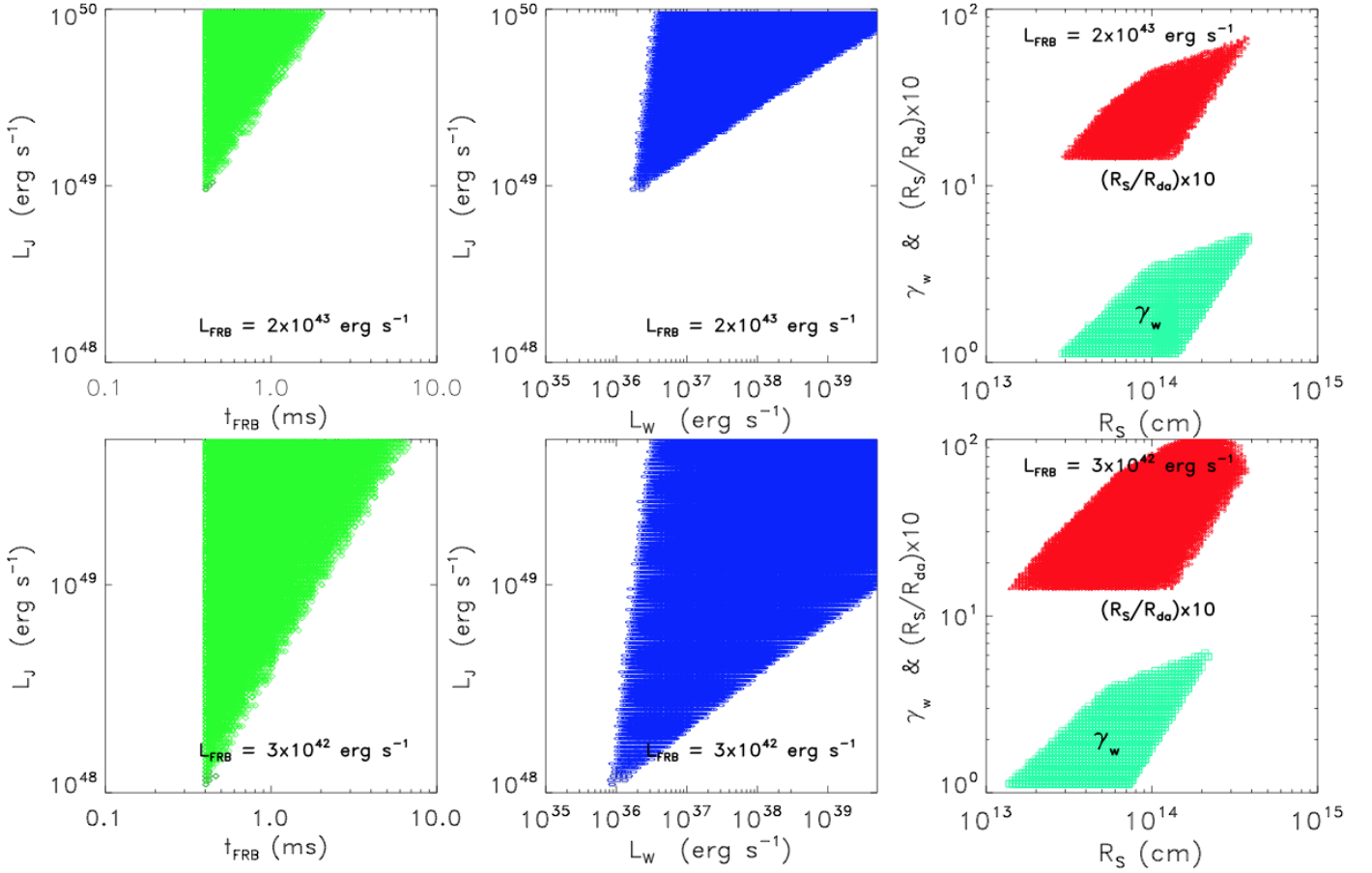


Figure 3. We show results of numerical calculations for FRB emission according to maser mechanisms operating in shocks that result from a relativistic jet of luminosity L_j colliding with a cold wind of luminosity L_w , both of which are produced by the same compact object. Each panel shows a pair of parameters that survive the constraint imposed by particle acceleration upstream of the shock front that shuts off the generation of coherent radiation. Constraints are placed on the particle acceleration time due to induced-Compton (IC) scatterings – $t_{\text{acc}}(R_s) > t_{\text{FRB}}/10$; where t_{FRB} is burst duration in observer frame which is calculated using eq. 49, and $t_{\text{acc}}(R_s)$, given by eq. 39, is particle acceleration time due to IC at the shock radius R_s (we note that our numerical calculation of t_{acc} includes nonlinear effects when the wave nonlinear parameter $a > 1$ whereas eq. 39 is valid only for $a \ll 1$). For the purpose of calculating upstream particle accelerations by the IC process, we have taken the observed, isotropic, FRB luminosity to be either $2 \times 10^{43} \text{ erg s}^{-1}$ (the top three panels) – the median luminosity of “non-repeating FRBs” is $\sim 10^{44} \text{ erg s}^{-1}$ (e.g. Luo et al. 2018; Ravi 2019) – or $3 \times 10^{42} \text{ erg s}^{-1}$ (bottom three panels), which is roughly the median luminosity for the bursts of the repeater FRB 121102 (e.g. Michilli et al. 2018; Hessels et al. 2019). We do not impose a prior on this luminosity as it is dependent on the details of the maser process whereas the focus of this paper is to provide general constraints that should apply to all maser mechanisms operating in shocks. We emphasize that the luminosity information is used only for the calculation of upstream particle acceleration and nothing else. We show in this figure the parameter space which yields the burst duration $t_{\text{FRB}} > 0.4 \text{ ms}$, and the peak frequency ν_B (given by eq. 50) greater than 0.4 GHz (which is the lowest frequency at which these bursts have been detected by CHIME – Amiri et al. 2019a, 2019b). The parameter search is cut off at $L_j > 10^{50} \text{ erg s}^{-1}$ and $L_w > 5 \times 10^{39} \text{ erg s}^{-1}$. The luminosity for the biggest magnetar flare we have ever observed (SGR 180620) was about $2 \times 10^{47} \text{ erg s}^{-1}$ in γ -rays (Hurley et al. 2005; Palmer et al. 2005), and the energy was smaller in relativistic outflows by a factor $\sim 10^2$ (Gelfand et al. 2005; Granot et al. 2006). The upper limit on L_j of $10^{50} \text{ erg s}^{-1}$ we have set in our numerical calculations is a factor $\sim 10^5$ larger than the luminosity of mildly-relativistic outflows for SGR 180620. The observed FRB frequency is taken to be the cyclotron frequency ν_B . What we find is that the maser-in-shock model for FRB radiation requires the isotropic luminosity of the relativistic jet responsible for the FRB radiation to be $\gtrsim 10^{49} \text{ erg s}^{-1}$ (top and bottom left and middle panels), and that means that the total outburst energy of the repeater FRB 121102 in just one year exceeds the magnetic field energy of a magnetar with surface field strength of $\sim 10^{15} \text{ G}$; we should point out that the high value of L_j is dictated entirely by the requirement that the emission is produced at a sufficiently large radius R_s and shock LF γ_{sw} (eq. 41), so as to avoid excessive particle acceleration upstream of the shock front due to IC, and at the same time produce burst duration $\gtrsim 0.4 \text{ ms}$; no constraint is placed as to how the maser mechanism operates and its efficiency. The top and bottom left panels show that the jet energy increases very rapidly with increasing burst duration. The top and bottom right panels show that the observed radiation is produced at a radius that is a few times larger than the deceleration radius of the jet, and the wind LF is between ~ 1 and 4 for reasons that are explained in §4.1.1. The upstream induced-Compton optical depth is included in these calculations, but it turns out to be a substantially weaker constraint than IC acceleration. The last point to note is that the maser-in-shocks model has no solutions for FRB luminosity $\gtrsim 10^{44} \text{ erg s}^{-1}$; there are solutions if we allow L_j to be larger than $\sim 10^{51} \text{ erg s}^{-1}$, but that poses problems for the total energetics.

$L_j \lesssim 10^{49} \text{ erg s}^{-1}$ (top left and middle panels of Fig. 3). And that is a serious problem for the maser-in-shock model for FRBs. The well studied repeater FRB 121102 has been observed for about 10 years, and $\gtrsim 10^2$ outbursts have been detected during the small observing time invested to following this object. The object has had numerous

outbursts with radio luminosity is GHz band of $\gtrsim 10^{43} \text{ erg s}^{-1}$. Each of these bursts require, according to the maser model, $L_j \gtrsim 10^{49} \text{ erg s}^{-1}$, and therefore, the total energy needed for outbursts in a year is at least 10^{48} erg if the efficiency for converting the magnetic energy to relativistic outflows is 100%. We know empirically that giant mag-

netar outbursts convert less than a few percent of magnetic energy to mildly-relativistic outflows⁵, and perhaps a much smaller fraction to ultra-relativistic jet that is invoked by maser-in-shocks models for FRB radio emission. This greatly exacerbates the energy problem – the energy requirement for maser-in-shocks model to support the activities of the FRB repeater for one year is $\gtrsim 10^{50}$ erg and that is hard for magnetic fields, even those as large as 10^{16} G, to provide. We note that the value of L_j in our calculations is dictated solely by the shock LF γ_{sw} and R_s such that the observed duration of bursts comes out to be of order a few ms, and not by any efficiency considerations.

The maser model yields no solution for FRB luminosity $\gtrsim 10^{44}$ erg s⁻¹ when the acceleration of upstream particles by IC scatterings shuts off the maser mechanism in less than 1 ms unless we consider the luminosity of the relativistic jet $L_j \gtrsim 10^{51}$ erg s⁻¹; L_j scales linearly with the FRB radio luminosity. We note that the analysis of ASKAP sample of bursts shows that there are FRBs with luminosity as high as $\sim 10^{46}$ erg s⁻¹ (Lu & Piro, 2019).

The main result of this sub-section is that it is highly unlikely that the FRB radiation is produced at a distance much larger than a few hundred neutron star radii. Particles in the region $10^9 \lesssim R_s \lesssim 10^{13}$ cm suffer very strong radiative acceleration which disrupts the photon generation process. The energy requirement for maser-in-shock models operating at $R_s \gtrsim 10^{13}$ cm is very challenging ($\gtrsim 10^{48}$ erg in ultra-relativistic outflows in one year for repeaters such as FRB 121102). For $R \lesssim 10^9$ cm, the strong magnetic field of a magnetar suppresses the induced-Compton scatterings and acceleration of particles by the electric field of FRB coherent radiation (discussed in the next sub-section). Therefore, the generation of coherent photons can proceed unimpeded close to the neutron star.

Although, almost all the discussions in this section have explicitly considered the scenario where FRB radiation is generated in shocks, the same physical considerations — acceleration of particles to high LF by the emergent radiation in the vicinity of the source region — apply to any other model for FRBs such as plasma maser type mechanism that operate far away from the neutron star surface and outside the light cylinder.

4.2 FRB radiation generation and propagation in a region of strong magnetic field

Photon-electron scattering cross-section is significantly modified in the presence of strong magnetic fields when the cyclotron frequency $\nu_B \gtrsim \nu$. The cross-section for an X-mode photon⁶ is (e.g. Canuto et al. 1971)

$$\sigma_x = \frac{\sigma_T}{2} \left[\frac{\nu^2}{(\nu + \nu_B)^2} + \frac{\nu^2}{(\nu - \nu_B)^2} \right], \quad (55)$$

⁵ The giant magnetar outburst of December 27, 2004 (SGR 180620) released 4×10^{46} erg in γ -rays (Hurley et al. 2005, Palmer et al. 2005) whereas the energy in mildly relativistic outflow, from radio observations, was estimated to be a few times 10^{44} erg (Gaensler et al. 2005, Gelfand et al. 2005, Granot et al. 2006). The peak luminosity for this burst, which was larger by a factor $\sim 10^2$ compared with the previous two most luminous SGRs, was $\sim 2 \times 10^{47}$ erg s⁻¹. The duration of the initial γ -ray spike, which carried most of the energy release, for all three giant SGR flares was 0.2s.

⁶ An X-mode is a linearly polarized EM wave with the direction of the wave electric field vector perpendicular to the plane of static magnetic field and the wave-vector.

and the cross-section when the wave electric field is not perpendicular to the static magnetic field is:

$$\sigma_{\parallel} = \sigma_T \left[\sin^2 \theta_{kB} + \frac{\cos^2 \theta_{kB}}{2} \left\{ \frac{\nu^2}{(\nu + \nu_B)^2} + \frac{\nu^2}{(\nu - \nu_B)^2} \right\} \right], \quad (56)$$

where the cyclotron frequency

$$\nu_B = \frac{qB}{2\pi mc}, \quad (57)$$

$\sin \theta_{kB} \approx \theta_{kB}$ is the dot product of unit vectors along the static magnetic field and wave electric field as measured in the electron rest frame, and ν is EM wave frequency also in the electron rest frame. These formulae for the cross-section apply only when the EM wave nonlinearity parameter $a_{\parallel} \equiv qE_{\parallel}/m\omega$ (see eq. 2) is much less than 1; E_{\parallel} is the component of wave electric vector amplitude along the static magnetic field. For the X-mode we are considering here, the angle between the wave electric field and the magnetic field is very close to $\pi/2$ (eq. 60), and $a_{\parallel} \ll 1$; this point is further addressed below (60).

We see from equation (39) that for $R \lesssim 10^{13}$ cm the timescale for particle acceleration due to induced-Compton scatterings are extremely short, provided that the cross-section for scattering a photon by an electron into an unoccupied state is not drastically smaller than σ_T . However, as we see from equation (55), σ_x is smaller than σ_T by a factor $(\nu_B/\nu)^2$ in the region of high magnetic field. Attenuation of O-modes⁷ by interactions with electrons in the medium in the vicinity of the source is also suppressed by a factor $\sim \theta_{kB}^{-2}$; modes with $\theta_{kB} \ll 1$ are unlikely to be able to escape the immediate vicinity of the source region intact.

Consider an X-mode generated at radius R_s (measured from the center of the host neutron star with strong magnetic field) such that $R_s \lesssim 10^7$ cm. It was shown by Lu et al. (2019) that the electric-vector of an X-mode traveling through a medium with non-uniform magnetic field rotates in such a way as to keep the wave-electric field pointing nearly perpendicular to the local magnetic field and the wave-vector as long as the plasma density is sufficiently large; the index of refraction of the medium for this mode is very close to unity, so the wave-vector does not rotate. The RMS angle $|\hat{\mathbf{E}}_{\text{w}} \times \hat{\mathbf{B}}|$ as the wave travels away from the source region is given by (Lu et al., 2019)

$$\theta_{kB} \approx \frac{2\pi c\nu}{R_B \omega_p^2} \quad (58)$$

where $\omega_p^2 = 4\pi q^2 n/m$ is the plasma frequency, n is the electron density and R_B is the radius of curvature of magnetic field lines at the current location of the wave at R ; $R_B \sim R/\theta$ at polar coordinate (R, θ) wrt the magnetic axis. Let us take the e^{\pm} density at R to be \mathcal{M} times the Goldreich-Julian density (Goldreich & Julian, 1968)

$$\begin{aligned} n &= \mathcal{M} n_{GJ} = \frac{\mathcal{M} \mathbf{B} \cdot \boldsymbol{\Omega}_{\text{ns}}}{2\pi qc} \approx \frac{\mathcal{M} B_{ns} \Omega_{ns}}{2\pi qc} \left(\frac{R_{ns}}{R} \right)^3 \\ &\approx 10^{13} \text{cm}^{-3} \mathcal{M} B_{ns,15} \Omega_{ns} \left(\frac{R_{ns}}{R} \right)^3, \end{aligned} \quad (59)$$

where Ω_{ns} is the angular velocity of the NS.

Substituting this into (58) we find

$$\theta_{kB} \sim 6 \times 10^{-11} \mathcal{M}^{-1} \nu_9 R_{B,8}^{-1} B_{NS,15}^{-1} \Omega_{ns}^{-1} (R/R_{ns})^3, \quad (60)$$

inside the freeze-out radius given by equation (61). The wave nonlinearity parameter along the magnetic field $a_{\parallel} \equiv qE_{\parallel}/(m\omega) =$

⁷ An O-mode is a linearly polarized EM wave with the direction of the wave electric field vector in the plane of static magnetic field and the wave-vector.

$qE\theta_{kB}/(mc\omega) \ll 1$ even out to $R/R_{ns} \sim 10^3$ or $R \sim 10^9$ cm, if $\mathcal{M} \sim 10^3$ ($R_B \sim R/\theta \sim 10^2 R$ in the magnetic polar-cap region). Therefore, it is appropriate to use equation (56) for X-mode scattering cross section even for bright FRBs.

The rotation of wave electric field ceases at a radius, called the freeze-out radius, where the plasma density becomes too small to be able to provide the current needed to rotate the wave electric vector. This occurs at a radius where (Lu et al., 2019)

$$\frac{\omega_p^2}{\omega^2} \sim \frac{ac}{\omega R_B} \implies \frac{R_{fo}}{R_{ns}} \sim 2 \frac{(\mathcal{M} B_{ns,15} \Omega_{ns})^{\frac{1}{2}}}{L_{43}^{-\frac{1}{4}}} \left[\frac{R_B}{R_{ns}} \right]^{\frac{1}{2}}; \quad (61)$$

R_B in this equation is calculated at R_{fo} . The FRB radiation might be produced along open magnetic field lines in the polar cap region which has an angular size of $\theta_{pc} = [\Omega_{ns} R_{ns}/c]^{1/2} \sim 5.8 \times 10^{-3} (R_{ns,6} \Omega_{ns})^{1/2}$ rad. Taking $\theta \sim \theta_{pc}$ and substituting $R_B \sim R_{fo}/\theta$ in equation (61) leads to

$$\frac{R_{fo}}{R_{ns}} \sim 400 \mathcal{M} B_{ns,15} (\Omega_{ns}/R_{ns,6})^{1/2} L_{43}^{-1/2}. \quad (62)$$

The angle θ_{kB} at the freeze-out radius is:

$$\theta_{kB}(R_{fo}) \sim 10^{-5} \mathcal{M} B_{NS,15} L_{43}^{-1} \Omega_{ns}^{1/2} R_{ns,6}^{-3/2} \nu_9. \quad (63)$$

Making use of equation (60) we find that the photon-electron scattering cross-section, in the strong magnetic field regime ($\omega_B \gg \omega$), when the wave electric field is not exactly perpendicular to the large scale magnetic field is

$$\sigma_{\parallel} \sim \sigma_T \theta_{kB}^2 \sim 2 \times 10^{-45} \text{ cm}^2 \frac{\nu_9^2}{\mathcal{M}^2 B_{ns,15}^2 \Omega_{ns}^2 R_{B,8}^2} \left(\frac{R}{R_{ns}} \right)^6, \quad (64)$$

as long as $\theta_{kB} > \nu/\nu_B$, which is the only case we are considering here.

The induced-Compton scattering optical depth in this case is

$$\tau_{ic} \approx \frac{3\sigma_{\parallel} n L \theta_s^2}{64\pi^2 R \nu^3 m}, \quad (65)$$

where $\theta_s = \min\{\ell_s/R, \gamma_s^{-1}\}$ is the angular size of the photon beam at R , ℓ_s is the transverse size of the FRB source from which photons are received at R , and γ_s is the LF of the FRB source. Making use of equations (59) & (64) we find the optical depth to IC for $R \lesssim R_{fo}$

$$\tau_{ic} \sim 10^{-7} \frac{L_{43} \ell_{s,4}^2}{\nu_9 R_{B,9}^2 \mathcal{M} B_{ns,15} \Omega_{ns,1}}. \quad (66)$$

The IC optical depth is less than unity at all radii in the NS magnetosphere at least out to the light cylinder.

Next, we look into particle acceleration and energy loss in the source region of the FRB pulse. In a strong magnetic field region, particle acceleration time for e^{\pm} plasma due to IC scattering is a slightly modified form of equation (39)

$$t_{acc} \sim \frac{256\pi^3 R^4 \nu^3 m^2 c^2}{3\sigma_{\parallel} \theta_s^2 L^2}. \quad (67)$$

Using equation (64) leads to the following expression for the acceleration time

$$t_{acc} \sim (10^{-5} \text{ s}) \frac{\nu_9 (B_{ns,15} \Omega_{ns,1} \mathcal{M} R_{B,9})^2}{L_{43}^2 \ell_{s,4}^2} \quad \text{for } R \lesssim R_{fo}. \quad (68)$$

According to the coherent curvature model of FRBs (Kumar et al. 2017; Lu & Kumar 2018), $\mathcal{M} \gtrsim 10^3$ and $\ell_s \sim 10^4$ cm, and so the IC acceleration time within the source region of FRBs is $\sim 10^{-5}$ s. This is longer than ℓ_s/c , the residency time of e^{\pm} in the source region, and hence the induced-Compton cannot adversely affect the generation of

FRB coherent radiation. In fact, our estimate of t_{acc} inside the source region is probably too small. This is because the electric field of the radiation is exactly perpendicular to the static magnetic field (X-mode polarization) within the source and e^{\pm} s are stuck in the lowest Landau level and have weaker than classically expected interaction with X-mode photons. It is also the case that the coherent curvature radiation requires a strong electric field along the static magnetic field. Particle acceleration time due to this electric field is of order 10^{-16} s (Kumar et al. 2017), and the electric force on e^{\pm} far exceeds any non-zero IC scattering force.

Particles outside the source region, at larger radii, are accelerated to $LF \sim \theta_s^{-1} \sim R/\ell_s \sim 10^3 R_7/\ell_{s,4}$ when $t_{acc} \ll t_{FRB}$; the FRB radiation becomes roughly isotropic in the particle rest frame when the LF approaches this value, and IC scattering force drops to zero. The total number of e^{\pm} in the magnetosphere of a magnetar of spin period 1 s is $\sim 4\pi \mathcal{M} n_{GJ} R^3 \sim 3 \times 10^{36} \mathcal{M}_3 B_{ns,15}$. Therefore, the energy lost by the FRB radiation as it travels through the NS magnetosphere is $\lesssim 2 \times 10^{33} \mathcal{M}_3$ erg (isotropic equivalent). This energy loss is a tiny fraction of the total energy of the FRB coherent radiation⁸.

The nonlinearity parameter for the FRB coherent radiation (described in §2) is $\sim 10^5$ at $R = 10^8$ cm. In the absence of the magnetic field of the magnetar, e^{\pm} exposed to this radiation would be accelerated to $LF \sim 10^{10}$. However, the strong magnetic field of a magnetar suppresses particle acceleration drastically, and the LF e^{\pm} s attain at $R = 10^8$ cm is close to unity⁹. Therefore, particle acceleration by the electric field of FRB radiation does not change the conclusion we arrived at regarding the loss of FRB energy as photons travel through the NS magnetosphere to arrive at Earth, i.e. the loss of energy is negligible.

The main result of this subsection is that a FRB source located within a few 10s of neutron star radii of a magnetar can withstand the enormous radiation forces. Moreover, little energy is lost as the radiation travels through the NS magnetosphere. The reason for this is entirely due to the strong magnetic field of a magnetar which suppresses scattering cross-section and the efficiency of particle acceleration, i.e. in the absence of a strong magnetic field a large fraction of FRB radiation energy would be imparted to particles along its path as the radiation travels away from the source.

5 CONCLUSIONS

We have investigated the effects of an intense FRB coherent radiation on plasma around the region where the radiation is produced. The pur-

⁸ One might worry that electrons and positrons accelerated to high LF could trigger a pair production avalanche, which can sap the energy from FRB radiation. However, e^{\pm} accelerated by FRB radiation are moving away from the neutron star, and thus see the NS surface emission highly red-shifted and not capable of pair production. Moreover, the photon density associated with pulsar nebula emission is $\lesssim 10 \text{ cm}^{-3}$, which is too small for launching pair cascade.

⁹ The angle between the electric field of radiation and the local magnetic field direction minus $\pi/2$, defined to be θ_{kB} , is given by eq. 60. Thus, the wave nonlinearity parameter along the magnetic field $a_{\parallel} \equiv qE\theta_{kB}/(mc\omega) \ll 1$ for $R \lesssim 10^8$ cm. And, therefore, e^{\pm} are accelerated along the magnetic field by the electric field of the FRB radiation to speeds much smaller than c throughout most of the NS magnetosphere. The acceleration of particles perpendicular to the static magnetic field when the cyclotron frequency (ω_B) is much larger than wave frequency ω is determined by a modified non-linearity parameter $a_{\perp} \equiv qE/(mc\omega_B)$, which is less than 1 for $R \lesssim 10^8$ cm. Therefore, the particle speed perpendicular to the magnetic field is also sub-relativistic even quite far from the NS surface; at $R = 10^9$ cm, $a_{\perp} \sim 10$ and e^{\pm} LF is $\sim 10^2$.

pose is to constrain source properties and the radiation mechanism for FRBs by using some fairly general physics considerations, and determine conditions that a successful model should satisfy. In particular, we calculate particle speed due to electric field of the radiation and the highly enhanced scattering (the induced-Compton scattering) by electrons and positrons of the coherent FRB radiation where each quantum state has an occupancy number of order 10^{35} . We find that electrons and protons are accelerated to very high LF due to these forces. This severely restricts some, otherwise, promising models for FRBs. One such class of models invokes relativistic shocks and maser type instability operating in the shock transition zone or downstream of the shock front.

We have shown that the coherent radiation traveling upstream of the shock front stirs up the plasma violently – e^\pm have LF greater than 30 due to the strong electric field of the radiation – even when the shock front is at a distance of 10^{13} cm from the FRB compact progenitor star (see §2). Furthermore, induced-Compton scatterings push the upstream plasma away with a large LF as long as the shock front radius is less than $\sim 10^{13}$ cm, thereby preventing particles from approaching and crossing the shock front to keep the generation of GHz radiation going.

At larger distances ($\gtrsim 10^{13}$ cm) these forces are fairly tame. However, maser-in-shock models require an excessively large amount of energy ($\gtrsim 10^{46}$ erg) in ultra relativistic outflows to produce a burst at a few GHz frequency with luminosity $\gtrsim 10^{43}$ erg s^{-1} , at these large distances (see §4.1.1); as a point of reference, the total energy in relativistic outflows in the biggest magnetar flare ever observed (SGR 180620) was estimated to be $\sim 10^{44}$ erg from late time radio observations (Gelfand et al. 2005; Granot et al. 2006). The total energy in relativistic jets for bursts produced by the repeater FRB 121102 in one year, for maser models, is required to be substantially larger than 10^{48} erg. This exceeds the energy in magnetic fields of a NS with strength 10^{15} G, and that is assuming an efficiency of 100% for converting magnetic energy to relativistic jets; the actual efficiency is perhaps no larger than 1% (§4.1.1).

If FRBs were to be associated with SGRs then that has consequences for the maser-in-shock models. The γ -ray photons from the SGR will be scattered by electrons upstream of the shock front heating them up. Whether the maser instability can survive this interaction is unclear. Let us consider that the SGR associated with a FRB released 10^{47} erg in γ -rays, and the γ -ray luminosity was 10^{48} erg s^{-1} ; the duration of the γ -ray pulse for SGR 180620 was about 0.1 s. The γ -ray pulse is ahead of the shock front, when it is at radius R , by the distance $\delta R \approx R/(2\gamma sw^2) \sim ct_{FRB}$. Upstream electrons will be heated to the temperature of γ -rays on a time scale of $t_{ic\gamma} \sim (1 \text{ ms}) R_{13}^2 / L_{\gamma,48}$. Considering this short time scale, and small Larmor radius ($\lesssim 5 \times 10^3$ cm), the upstream particles would have anisotropic velocity distribution as they enter the shock front, and that could affect the instability.

Stimulated Raman and Brillouin scatterings can also attenuate the FRB radiation. The stimulated Raman process has been calculated by many people e.g. Gangadhara & Krishan (1992), Thompson et al. (1994), Levinson & Blandford (1995). Lyubarsky & Ostrovska (2016) considered Raman scatterings in the context of stellar coronae model for FRBs and concluded that it does not provide more severe constraint on the propagation of FRB radiation than the induced-Compton scatterings. However, implications of stimulated Raman and Brillouin scatterings for the more recent models for FRBs needs to be investigated.

We have shown in §4.2 that the FRB radiation source operating in a region of very strong magnetic field (where the cyclotron frequency is much larger than the FRB radio wave frequency) allevi-

ates these problems; the radiation forces are weaker in the presence of strong magnetic field, and the plasma in the FRB source region is not dispersed quickly. One of the reasons for this is that the interaction cross-section between e^\pm and X-mode photons is highly reduced in the presence of a strong magnetic field. The coherent curvature (“antenna”) model for FRBs requires very strong magnetic field for its successful operation (Kumar et al. 2017; Lu & Kumar 2018). It is shown in §4.2 that the source survives the radiative forces, and radiation traveling through the NS magnetosphere suffers negligible loss of energy.

6 ACKNOWLEDGMENTS

We thank the referee, Roger Blandford, for helpful comments and suggestions. WL acknowledges useful discussions with Lorenzo Sironi and Brian Metzger on the physics of synchrotron instability, with Ben Margalit on wind nebulae near magnetars, and we thank Bing Zhang for comments and suggestions. WL is supported by the David and Ellen Lee Fellowship at Caltech.

REFERENCES

- Amiri, M. et al. 2019a, *Nature* 566, 230
 Amiri, M. et al. 2019b, *Nature* 566, 235
 Bannister, K.W. et al. 2017, *ApJL* 841, L12
 Bannister, K.W. et al. 2019, *Science* 365, 565
 Blandford, R. D. 1973, *A&A* 26, 161
 Blandford, R.D. & Scharlemann, E.T. 1975, *A&SS* 36, 303,
 Blandford, R.D. & Scharlemann, E.T. 1976, *MNRAS* 174, 59
 Chatterjee, S. et al. 2017, *Nature* 541, 58
 Canuto, V., Lodenquai, J., Ruderman, M., 1971, *Physical Review D*, 3, 2303
 Cordes, J.M., Wasserman, I., Hessels, J.W.T., Lazio, T.J.W., Chatterjee, S. and Wharton, R.S. 2017, *ApJ* 842, 35
 Cordes J. M., Chatterjee S., 2019, *ARA&A*, 57, 417
 Farah et al. 2018, *MNRAS* 478, 1209
 Gaensler, B.M. 2005, *Nature* 434, 1104
 Gangadhara, R.T. & Krishan, V., *MNRAS* 1992, 256, 111
 Gajjar, V. et al. 2018, *ApJ* 863, 2
 Gelfand, J.D. 2005, *ApJ* 634, L89
 Goldreich, P., and Julian, W. H. 1969, *Ap. J.*, 157,869
 Granot, J. et al. 2006, *ApJ* 638, 391
 Granot, J., Komissarov, S.S., Spitkovsky, A. 2011, *MNRAS* 411, 1323
 Hessels, J.W.T. et al. 2019, *ApJL* 876, L23
 Hurley, K. et al. 2005, *Nature* 434, 1098
 Lyubarsky, Y. & Ostrovska, S. 2016, *ApJ* 818, 74
 Katz, J.I. 2018, *Progress in Particle and Nuclear Physics* 103, 1
 Kennel, C.F. & Coroniti, F.V. 1984, *ApJ* 283, 694
 Kocz, J. et al. 2019, [arXiv:1906.08699](https://arxiv.org/abs/1906.08699)
 Kumar, P., Lu, W. and Bhattacharya, M. 2017, *MNRAS* 468, 2726
 Kumar, P., Zhang, B. 2015, *Physics Reports* 561, 1
 Law, C.J. et al., 2017, *ApJ* 850, 76
 Levinson, A. & Blandford, R.D. 1995, *MNRAS* 274, 717
 Lorimer, D.R., Bailes, M., McLaughlin, M.A., Narkevic, D.J., Crawford, F., 2007, *Science* 318, 777
 Lu, W. and Kumar, P. 2018, *MNRAS* 477, 2470
 Lu, W., Kumar, P. and Narayan, R. 2019, *MNRAS* 483, 359
 Lu, W. and Piro, A.L. 2019, *ApJ* 883, 40
 Luo R., Lee K., Lorimer D.R., Zhang B. 2018, *MNRAS*, 481, 2320

- Lyubarsky, Y. 2008, *ApJ* 682, 1443
Marcote, B. et al. 2017, *ApJ* 834, L8
Main, R. et al. 2018, *Nature* 557, 522
Melrose, D.B. 1971, *Astrophysics & Space Science* 13, 56
Metzger, B.D., Berger, E., and Margalit, B. 2017, *ApJ* 841, 14
Metzger, B.D., Margalit, B., and Sironi, L. 2019, *MNRAS* 485, 4091
Michilli, D. et al., 2018, *Nature* 553, 182
Osłowski, S. et al. 2019, *MNRAS* 488, 868
Palmer, D.M. et al. 2005, *Nature* 434, 1107
Petroff, E., Barr, E.D., Jameson, A., Keane, E.F., Bailes, M., Kramer, M., Morello, V., Tabbara, D. and van Straten, W., 2016, *Pub. Astro. Soc. of Australia*, 33, e045
Petroff E., Hessels J. W. T., Lorimer D. R., 2019, *A&ARv*, 27, 4
Plotnikov I., Sironi L., 2019, *MNRAS*, 485, 3816
Ravi, V. 2019a, *MNRAS* 482, 1966
Ravi, V. 2019b, [arXiv:1907.06619](https://arxiv.org/abs/1907.06619)
Ravi, V. et al. 2019, *Nature*, [arXiv:1907.01542](https://arxiv.org/abs/1907.01542)
Shannon, R.M. et al. 2018, *Nature* 562, 386
Spitler, L.G. et al. 2014, *ApJ* 790, 101
Spitler, L.G. et al. 2016, *Nature* 531, 202
Tendulkar, S.P. et al. 2017, *ApJ* 834, L7
Thompson, C., Blandford, R.D., Evans, C. & Phinney, E.S. 1994, *ApJ* 422, 304
Thornton, D. et al. 2013, *Science* 341, 53
Wilson, D.B. & Rees, M.J. 1978, *MNRAS* 185, 297
Yang Y.-P., Zhang B., 2018, *ApJ*, 868, 31